A&A 646, L9 (2021)
https://doi.org/10.1051/0004-6361/202040177

Astronomy & Astrophysics

LETTER TO THE EDITOR

A study of C_4H_3N isomers in TMC-1: Line by line detection of $HCCCH_2CN$*

N. Marcelino[1], B. Tercero[2,3], M. Agúndez[1], and J. Cernicharo[1]

[1] Grupo de Astrofísica Molecular, Instituto de Física Fundamental, CSIC, C/ Serrano 123, 28006 Madrid, Spain
e-mail: nuria.marcelino@csic.es
[2] Observatorio Astronómico Nacional (IGN), C/ Alfonso XII 3, 28014 Madrid, Spain
[3] Observatorio de Yebes (IGN), Cerro de la Palera s/n, 19141 Yebes, Guadalajara, Spain

Received 19 December 2020 / Accepted 20 January 2021

ABSTRACT

We present Yebes 40 m telescope observations of the three most stable C_4H_3N isomers towards the cyanopolyyne peak of TMC-1. We have detected 13 transitions from CH_3C_3N (A and E species), 16 lines from CH_2CCHCN, and 27 lines (*a*-type and *b*-type) from $HCCCH_2CN$. We thus provide a robust confirmation of the detection of $HCCCH_2CN$ and CH_2CCHCN in space. We have constructed rotational diagrams for the three species and obtained rotational temperatures between 4 and 8 K as well as similar column densities for the three isomers, in the range $(1.5–3) \times 10^{12}$ cm^{-2}. Our chemical model provides abundances of the order of the observed ones, although it overestimates the abundance of CH_3CCCN and underestimates that of $HCCCH_2CN$. The similarity of the observed abundances of the three isomers suggests a common origin, most probably involving reactions of the radical CN with the unsaturated hydrocarbons methyl acetylene and allene. Studies of reaction kinetics at low temperatures and further observations of these molecules in different astronomical sources are needed to draw a clear picture of the chemistry of C_4H_3N isomers in space.

Key words. astrochemistry – ISM: abundances – ISM: clouds – ISM: individual objects: TMC-1 – ISM: molecules – line: identification

1. Introduction

Three C_4H_3N isomers have been detected in space to date. They are, in order of increasing energy, methylcyanoacetylene (CH_3C_3N), cyanoallene (CH_2CCHCN), and propargyl cyanide ($HCCCH_2CN$). Our knowledge of C_4H_3N isomers in the interstellar medium is the result of an auspicious multidisciplinary history, with contributions from theoretical calculations, laboratory experiments, and astronomical observations. The presence of cyanoallene in cold interstellar clouds was predicted by Balucani et al. (2000, 2002) based on crossed molecular beam experiments and ab initio calculations that indicated that the reaction of CN and CH_3CCH would produce CH_3C_3N, already detected in TMC-1 (Broten et al. 1984), and CH_2CCHCN in nearly equal amounts. Laboratory experiments indeed showed that the reaction CN + CH_3CCH is rapid at low temperatures (Carty et al. 2001). These results motivated an astronomical search for cyanoallene in TMC-1, which was accomplished using the Green Bank Telescope (GBT; Lovas et al. 2006) and the Effelsberg 100 m telescope (Chin et al. 2006).

In their combined crossed beam and ab initio study, Balucani et al. (2000, 2002) also studied the reaction between CN and CH_2CCH_2 (allene), a non-polar metastable isomer of CH_3CCH that is thought to also be present in cold interstellar clouds. These authors found that the reaction should be rapid at low temperatures, something that was confirmed by Carty et al. (2001), producing cyanoallene and the third C_4H_3N isomer: $HCCCH_2CN$. This isomer was not detected in TMC-1 by Lovas et al. (2006), although it was later found towards this same source during a centimetre line survey with the GBT (McGuire et al. 2020). The detection of propargyl cyanide in TMC-1 by these authors relied on four individual lines detected at a modest signal-to-noise ratio (S/N) and was supported by the line stacking of 68 transitions.

Here we present an independent and robust detection of $HCCCH_2CN$ in TMC-1, with ten lines detected with S/Ns above 10 plus 12 lines detected above 3σ, together with observations of the two other C_3H_4N isomers, CH_3C_3N and CH_2CCHCN. The presence of the latter is confirmed by the detection of a significant number of rotational lines. The high sensitivity and number of lines detected allow us to derive precise abundances for the three isomers in a coherent and systematic way and to revisit the chemistry of C_3H_4N isomers in TMC-1.

2. Observations

The data presented here are part of a deep spectral line survey in the *Q* band towards TMC-1 that was performed at the Yebes 40 m radio telescope[1] (de Vicente et al. 2016), located at an altitude of 990 m near Guadalajara (Spain). The observed position corresponds to the cyanopolyyne peak (CP) in TMC-1, at $\alpha_{J2000} = 4^h41^m41.9^s$ and $\delta_{J2000} = +25°41'27.0''$. We

* Based on observations with the 40 m radio telescope of the National Geographic Institute of Spain (IGN) at Yebes Observatory (projects 19A003 and 20A014). Yebes Observatory thanks the ERC for funding support under grant ERC-2013-Syg-610256-NANOCOSMOS.

[1] http://rt40m.oan.es/rt40m_en.php

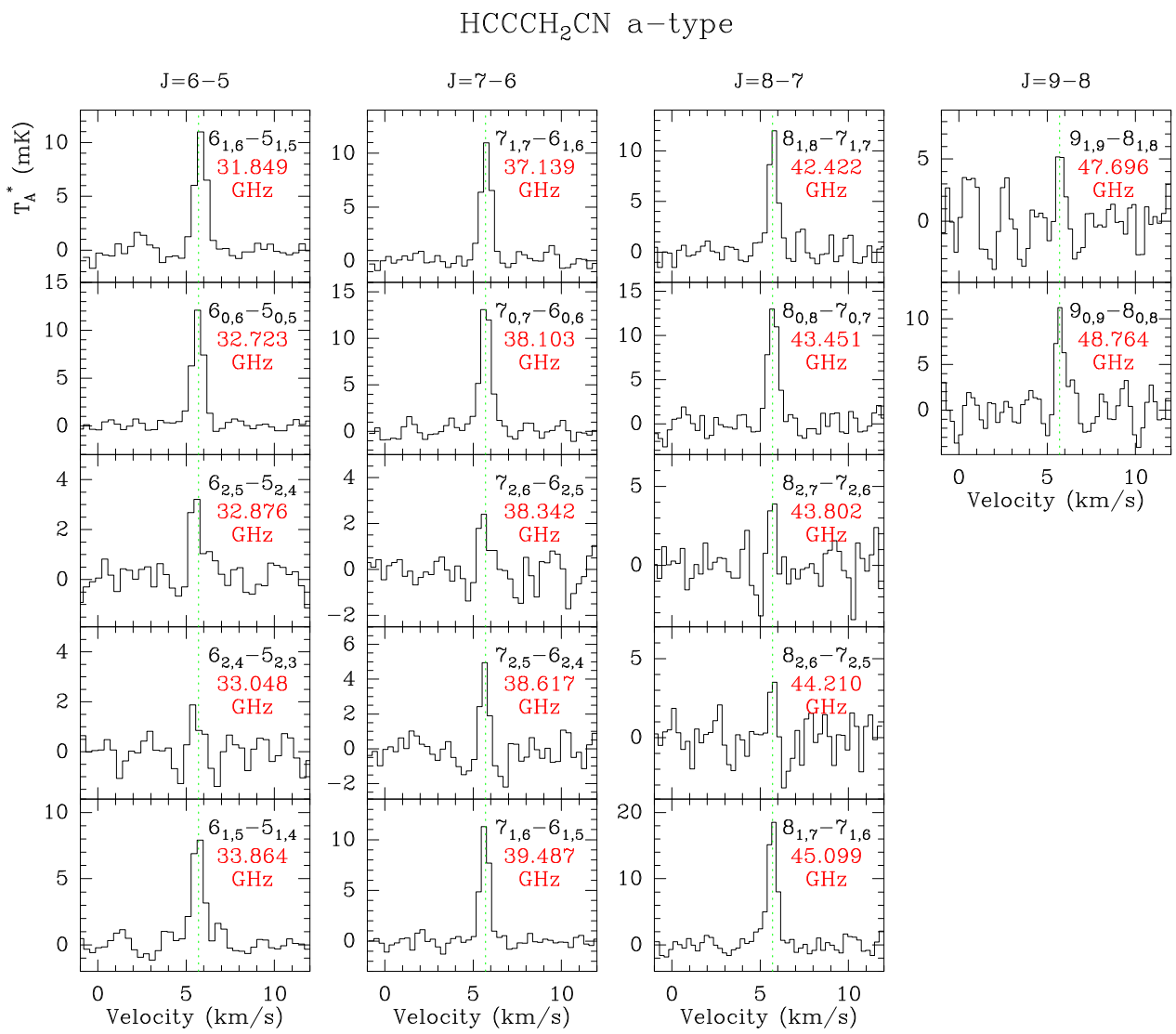

Fig. 1. Observed lines of $HCCCH_2CN$ (*a*-type) towards TMC-1 (CP). The vertical dashed green line marks a radial velocity of 5.7 km s^{-1}.

covered the full *Q* band at the 40 m telescope, between 31.1 GHz and 50.4 GHz, using the recently installed NANOCOSMOS high-electron-mobility transistor (HEMT) *Q* band receiver (Tercero et al. 2021) and the fast Fourier transform spectrometers (FFTSs) with 8×2.5 GHz bands per lineal polarization, which allow a simultaneous scan of a bandwidth of 18 GHz at a spectral resolution of 38 kHz (~0.27 km s^{-1}). We observed two setups at different central frequencies in order to fully cover the lower and upper frequencies allowed by the *Q* band receiver and to check for spurious signals and other technical artefacts.

The observations were performed in several sessions, between November 2019 and February 2020, using the frequency switching technique with a frequency throw of 10 MHz. The intensity scale in the spectra obtained is T_A^*, the antenna temperature corrected for atmospheric absorption and spillover losses, which was calibrated using two absorbers at different temperatures and the atmospheric transmission model (ATM, Cernicharo 1985; Pardo et al. 2001). Pointing and focus were checked every hour through pseudo-continuum observations (see e.g., de Vicente et al. 2016; Tercero et al. 2020) of the SiO $J = 1-0$, $v = 1$ maser emission towards the O-rich evolved star IK Tau, which is close to the target source. The pointing errors were always found within 2–3″. System temperatures were in the range 50–250 K depending on the frequency, the particular weather conditions of each observing session (from 5 mm to 10 mm of precipitable water vapour), and the elevation of the source (from 15° to 80°). The final rms obtained is in the range 0.5–1 mK, rising up to 3 mK at the highest frequencies. The main beam efficiency of the Yebes 40 m telescope ranges from 0.6 at 32 GHz to 0.43 at 49 GHz, and the half power beamwidth (HPBW) ranges from 55″ at 32 GHz to 37″ at 49 GHz. All the data were reduced and analysed using the GILDAS[2] software.

3. Results

The high sensitivity of this line survey allowed the detection of $HCCCH_2CN$ towards TMC-1 through 17 *a*-type lines up to quantum numbers $J = 9-8$ and $K_a = 0, 1, 2$ ($E_u \leq 13$ K), ten of which showed an $S/N > 10$. In addition, we detected ten *b*-type lines harbouring hyperfine structures. These lines are shown in Figs. 1 and 2 and are listed in Table A.1. Line identification was performed using the MADEX catalogue (Cernicharo 2012, see Table A.1), which also includes predictions for the hyperfine structure. This detection confirms the presence of this

[2] http://www.iram.fr/IRAMFR/GILDAS/

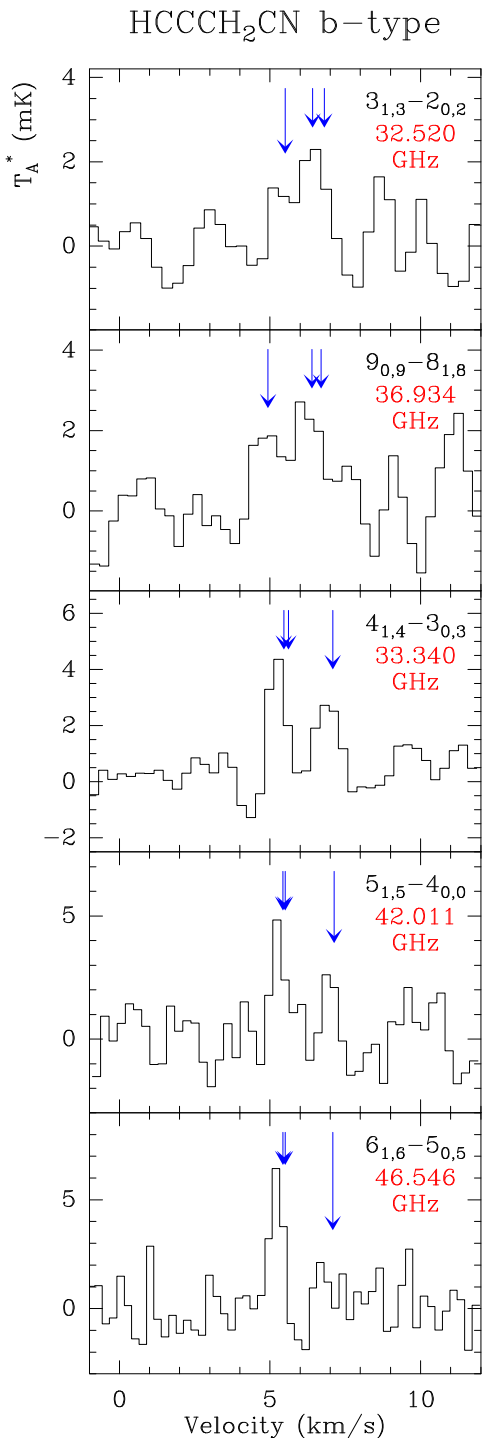

Fig. 2. Observed lines of $HCCCH_2CN$ (*b*-type) towards TMC-1 (CP). Blue arrows show the position of the three strongest hyperfine components. The velocity axis refers to the frequency result of collapsing the hyperfine structure.

species in space, recently claimed for the first time in TMC-1 by McGuire et al. (2020) using the GBT. These authors presented a 5σ signal (18σ in the response impulse function) obtained by an intensity and noise-weighted average ('stack') of the data at the expected frequencies of the $HCCCH_2CN$ lines that could be present within the noise level. It is worth noting that our 40 m survey of TMC-1 in the *Q* band is complementary to that performed with the GBT between 8 GHz and 30 GHz. Although most of the individual lines of $HCCCH_2CN$ are below the detection limit of the GBT data, four of them are detected at $1-3\sigma$ levels. Thanks to the high spectral resolution of these data (1.4 kHz), McGuire et al. (2020) distinguished three cloud components in the line profiles (see Fossé et al. 2001 for a detailed analysis of the velocity structure of this source).

In this work, a single Gaussian function was fitted to the $HCCCH_2CN$ line profiles to obtain the observed line parameters (see Table A.1). We derived a V_{LSR} = (5.70 ± 0.09) km s^{-1} and a line width (Δv, full width at half maximum) of (0.66 ± 0.18) km s^{-1}. The former is slightly different from the value (5.83 ± 0.01) km s^{-1} obtained by Cernicharo et al. (2020a) from Gaussian fits to the 50 lines of HC_5N and its ^{13}C and ^{15}N isotopologues detected in our line survey. It should be noted that we have a larger uncertainty due to the lower number of transitions and the weakness of some of the lines as compared to HC_5N, in particular the *b*-type transitions.

We also detected the other two C_4H_3N isomers, CH_2CCHCN and CH_3CCCN, using frequencies from the MADEX catalogue (Cernicharo 2012, see Table A.1). The 16 lines of CH_2CCHCN detected in our line survey are shown in Fig. A.1 and are listed in Table A.1. All of them are detected above a 10σ level. This species was previously identified in TMC-1 through four lines between 20 GHz and 26 GHz (Lovas et al. 2006). Here we report the first detection of lines of CH_2CCHCN above 30 GHz in TMC-1. Kaifu et al. (2004) did not detect lines above the noise limit at the CH_2CCHCN frequencies in the line survey they performed between 8.8 GHz and 50 GHz with the Nobeyama 45 m telescope. As we mentioned in previous works (Cernicharo et al. 2020a,b,c; Marcelino et al. 2020), the sensitivity of our observations is a factor of 5−10 better than that of Kaifu et al. (2004) at the same frequencies. The V_{LSR} for the CH_2CCHCN lines, derived by fitting a single Gaussian, is (5.66 ± 0.03) km s^{-1}, which is similar, within errors, to the one obtained for $HCCCH_2CN$. The isomer CH_3CCCN, a well-known species in TMC-1 (Broten et al. 1984; Kaifu et al. 2004), has also been identified in our line survey through ten strong lines (J_u from 8 to 12 and $K = 0, 1$) plus five $K = 2$ lines ($E_u > 29$ K) that were tentatively detected (see Fig. A.2 and Table A.1). These lines show a V_{LSR} of (5.80 ± 0.02) km s^{-1}, which matches that observed for HC_5N.

We can estimate rotational temperatures (T_{rot}) and molecular column densities (N) for the detected species by constructing rotational diagrams (see e.g., Goldsmith & Langer 1999). This analysis assumes the Rayleigh-Jeans approximation, optically thin lines, and local thermodynamic equilibrium conditions. The equation that derives the total column density under these conditions can be re-arranged as

$$\ln\left(\frac{8\pi k_B \nu^2 \int T_{MB} dv}{hc^3 A_{ul} g_u b}\right) = \ln\left(\frac{N}{Q_{rot}} \frac{T_{rot} - T_{bg}}{T_{rot}}\right) - \frac{E_u}{k_B T_{rot}}, \quad (1)$$

where g_u is the statistical weight in the upper level, A_{ul} is the Einstein *A*-coefficient for spontaneous emission, Q_{rot} is the rotational partition function (which depends on T_{rot}), E_u is the upper level energy, ν is the frequency of the transition, b is the dilution factor, and T_{bg} is the cosmic microwave background radiation temperature. We assumed a source diameter of 80″ (see Fossé et al. 2001). The first term of Eq. (1), which depends only on spectroscopic and observational line parameters, is plotted as a function of E_u/k_B for the different lines detected. Thus, T_{rot} and N can be derived by performing a linear least squares fit to the points (see Fig. A.3).

Results for T_{rot} and N using the population diagram procedure are shown in Table 1 and Fig. A.3. The uncertainties were

Table 1. Derived rotational temperatures (T_{rot}) and column densities (N) for the C_4H_3N isomers towards TMC-1 (CP).

Species	T_{rot} (K)	N (cm^{-2})
$HCCCH_2CN$	4 ± 1	$(2.8 \pm 0.7) \times 10^{12}$
CH_2CCHCN	5.5 ± 0.3	$(2.7 \pm 0.2) \times 10^{12}$
A-CH_3CCCN	6.7 ± 0.2	$(9.7 \pm 0.3) \times 10^{11}$
E-CH_3CCCN	8.2 ± 0.6	$(7.7 \pm 0.5) \times 10^{11}$

calculated using the statistical errors given by the linear least squares fit for the slope and the intercept. The individual errors of the data points are those derived by taking into account the uncertainty obtained in the determination of the observed line parameters (see Table A.1). For $HCCCH_2CN$ (a-type transitions) and CH_2CCHCN, different hyperfine structure components of the same $(J_{K_a,K_c})_u$–$(J_{K_a,K_c})_l$ transition are blended in a single line. Thus, to correctly determine T_{rot} and N, the Einstein A-coefficient for spontaneous emission and the statistical weight were assumed as the weighted average values of the sum of the hyperfine components, and the rotational partition function was calculated using this value for the statistical weight of each $(J_{K_a,K_c})_u$–$(J_{K_a,K_c})_l$ transition. For CH_3CCCN, we built independent rotational diagrams for each symmetry state, A and E.

We obtained rotational temperatures between 4 and 8 K for the three isomers (see Table 1), indicating they are subthermally excited, like most of the species in this region (see e.g., Cernicharo et al. 2020a,c; Marcelino et al. 2020). For the column density, we derived very similar values for the three isomers, in the range $(1.5–3) \times 10^{12}$ cm^{-2}.

4. Discussion

The chemistry of C_4H_3N isomers in cold molecular clouds was discussed by Balucani et al. (2000), and more specifically by Balucani et al. (2002), based on crossed molecular beam experiments and ab initio calculations. In these studies, it was pointed out that reactions of the CN radical with methyl acetylene and allene are barrier-less and exothermic when producing CH_3C_3N and CH_2CCHCN in the methyl acetylene reaction, and CH_2CCHCN and $HCCCH_2CN$ in the reaction involving allene. Indeed, the reactions of CN with CH_3CCH and CH_2CCH_2 were measured to be rapid at low temperatures (Carty et al. 2001). This chemical scheme was implemented in a chemical model by Quan & Herbst (2007) to explain the abundance of cyanoallene in TMC-1. Later on, Abeysekera et al. (2015) measured the product branching ratios of the reaction between CN and methyl acetylene at low temperatures using a chirped-pulse uniform flow and found that HC_3N is the major product, while CH_3C_3N accounts for 22% of the products and CH_2CCHCN is not formed. These results are in contrast with those obtained from crossed molecular beam experiments (Huang et al. 1999; Balucani et al. 2000, 2002), where CH_2CCHCN is observed as a product of the CN + CH_3CCH reaction. Therefore, the most stable isomer, CH_3C_3N, can be formed in the reaction of CN and methyl acetylene, the second most stable isomer, CH_2CCHCN, can be formed when CN reacts with CH_2CCH_2 – and perhaps also with CH_3CCH, depending on whether one gives credit to the chirped-pulse uniform flow experiment or to the crossed molecular beam ones – and the least stable isomer, $HCCCH_2CN$, can only be formed in the reaction between CN and allene. These neutral-neutral reactions involving CN are therefore likely routes to the three C_4H_3N isomers in cold interstellar clouds such as TMC-1, where abundant CN, CH_3CCH, and probably CH_2CCH_2 (non-polar and thus cannot be detected at radio wavelengths) are present. Moreover, the presence of $HCCCH_2CN$ (and perhaps also CH_2CCHCN) can be used as a proxy of the non-polar C_3H_4 isomer allene since this isomer is only formed from CH_2CCH_2 in the aforementioned reactions of CN.

In light of the recent discovery of $HCCCH_2CN$ in TMC-1 and the observational study of the three C_4H_3N isomers presented here, we carried out chemical model calculations to review the chemistry of these species in cold clouds and evaluate whether the mechanism proposed by Balucani et al. (2002) is in agreement with observations. We adopted typical parameters of cold dark clouds, namely a gas kinetic temperature of 10 K, a volume density of H nuclei of 2×10^4 cm^{-3}, a visual extinction of 30 mag, a cosmic-ray ionization rate of H_2 of 1.3×10^{-17} s^{-1}, and the so-called low-metal elemental abundances (Agúndez & Wakelam 2013). We used the chemical network ssRATE12 from the UMIST database (McElroy et al. 2013), updated to include the C_4H_3N isomers CH_2CCHCN and $HCCCH_2CN$. The reactions

$$\begin{aligned} CN + CH_3CCH &\rightarrow HCN + CH_2CCH, && (2a)\\ &\rightarrow HC_3N + CH_3, && (2b)\\ &\rightarrow CH_3C_3N + H, && (2c)\\ &\rightarrow CH_2CCHCN + H, && (2d) \end{aligned}$$

$$\begin{aligned} CN + CH_2CCH_2 &\rightarrow CH_2CCHCN + H, && (3a)\\ &\rightarrow HCCCH_2CN + H && (3b) \end{aligned}$$

are included with the rate constants measured by Carty et al. (2001). For the branching ratios of reaction (2), we used either the values measured in the chirped-pulse uniform flow experiment by Abeysekera et al. (2015) – 12%, 66%, 22%, and 0% for channels (a), (b), (c), and (d), respectively – or the values suggested by the crossed molecular beam experiments and quantum chemical calculations carried out by Balucani et al. (2000) – 50% for channels (c) and (d). For reaction (3), we adopted branching ratios of 90% and 10% for channels (a) and (b), respectively, based on the quantum chemical calculations by Balucani et al. (2002). The destruction processes of CH_2CCHCN and $HCCCH_2CN$ are assumed to be the same as those of CH_3C_3N, which are basically reactions with abundant cations.

The calculated abundances of the three C_4H_3N isomers are shown as a function of time in Fig. A.4. It is seen that the three isomers reach their maximum abundance at early times, in the range $(1–4) \times 10^5$ yr, with CH_3C_3N being the most abundant and $HCCCH_2CN$ being the least abundant. According to the chemical model, the formation of CH_3C_3N occurs through two routes. The first and main route involves the dissociative recombination of the precursor ion $CH_3C_3NH^+$ with electrons, and it is responsible for the larger calculated abundance of CH_3C_3N relative to the two other isomers. A second, minor route is provided by reaction (2c). Cyanoallene is formed through reaction (3), with reaction (2c) contributing to the same level if channel (2d) is assumed to be open. Propargyl cyanide is exclusively formed through reaction (3), with a lower abundance because it is formed with a branching ratio of just 10%. The impact of using the branching ratios for reaction (2) of Balucani et al. (2000) or those of Abeysekera et al. (2015) is modest, with the main effect being a change of less than a factor of two in the abundance of CH_2CCHCN (see Fig. A.4).

The fact that the observed abundances of the three isomers are remarkably similar provides clues regarding the underlying chemical processes at work. For example, the route to CH_3C_3N from the precursor ion $CH_3C_3NH^+$ is probably overestimated in the chemical model, as indicated by the excessively large abundance calculated for this species. It has become clear in recent years that the dissociative recombination of polyatomic ions usually results in a much larger fragmentation than previously believed (Larsson et al. 2012), meaning that it would not be strange if CH_3C_3N were a minor product in the dissociative recombination of $CH_3C_3NH^+$. The low branching ratio adopted for $HCCCH_2CN$ formation in reaction (3) based on calculations by Balucani et al. (2002) also seems to be in conflict with the observational finding of similar abundances for CH_2CCHCN and $HCCCH_2CN$. It would be very interesting to measure the product branching ratios for the reaction of CN with allene, as was done for $CN + CH_3CCH$ (Abeysekera et al. 2015), to shed light on the formation routes of these two metastable C_4H_3N isomers. This would also allow us to put tight constraints on the abundance of allene in cold dense clouds.

In summary, the similar abundances observed for the three C_4H_3N isomers favour a common origin through reactions (2) and (3), with similar branching ratios in the latter reaction. If this scenario is correct, we can conclude that allene is as abundant as methyl acetylene in TMC-1. This is indeed predicted by the chemical model, where CH_3CCH and CH_2CCH_2 are mostly formed during the dissociative recombination of the $C_3H_7^+$ ion (Larsson et al. 2005), with similar branching ratios assumed for the two C_3H_4 isomers.

In addition to the three C_4H_3N isomers and the well-known species HC_3N and CH_2CHCN, Balucani et al. (2000) predicted the presence of *c*-C_6H_5CN and the C_5H_5N isomer $CH_2CC(CN)CH_3$ in cold interstellar clouds. It is worth noting that all these species, with the exception of $CH_2CC(CN)CH_3$, have been identified in TMC-1 (see McGuire et al. 2018 for the detection of cyanobenzene) and are also present in our survey. Another −CN species, cyanocyclopentadiene (*c*-C_5H_5CN), has recently been detected in this source (McCarthy et al. 2021). A complete study of the molecular rings *c*-C_6H_5CN and *c*-C_5H_5CN in our data will be published elsewhere. We searched in our data for the two C_5H_5N isomers CH_3CH_2CCCN and $CH_3CHCCHCN$ by performing a line stacking analysis (see e.g., Cuadrado et al. 2016; Loomis et al. 2021). We added spectra at the expected frequency of several lines from these species that could be present within the noise level. More concretely, we considered *a*-type transitions sharing similar upper level energies, up to 15 K, and Einstein coefficients. All spectra, on a local standard of rest (LSR) velocity scale, are re-sampled to the same velocity channel resolution before stacking. Figure A.5 shows the spectra obtained following this method. While there is no evidence for the presence of CH_3CH_2CCCN in our data, the stacked spectrum of $CH_3CHCCHCN$ shows a 2σ signal at the systemic velocity of the source. An observational effort at lower frequencies has to be undertaken to confirm the presence of $CH_3CHCCHCN$ in space.

5. Conclusions

Using a very sensitive line survey of TMC-1 in the *Q* band, we have detected multiple transitions of the three C_4H_3N isomers CH_3C_3N, CH_2CCHCN, and $HCCCH_2CN$. The presence of this third isomer in TMC-1 is supported by 27 observed individual lines. We have constructed rotational diagrams for the three species and obtained similar rotational temperatures and column densities for the three isomers, in the ranges of 4−8 K and $(1.5–3)\times10^{12}$ cm^{-2}, respectively. The observed abundances of the three isomers in TMC-1 suggest a similar chemical origin based on reactions of the radical CN with the isomers CH_3CCH and CH_2CCH_2. There are still uncertainties in the network of reactions related to these species since our chemical model overestimates the abundance of CH_3C_3N and underestimates the production of $HCCCH_2CN$. Further studies of these isomers in other sources could help in clarifying their chemical formation pathways.

Acknowledgements. We acknowledge funding support from the European Research Council (ERC Grant 610256: NANOCOSMOS). We also thank the Spanish MICIU for funding support under grants AYA2016-75066-C2-1-P, PID2019-106110GB-I00, PID2019-107115GB-C21, and PID2019-106235GB-I00. M.A. thanks MICIU for grant RyC-2014-16277.

References

Abeysekera, C., Joalland, B., Ariyasingha, N., et al. 2015, J. Phys. Chem. Lett., 6, 1599
Agúndez, M., & Wakelam, V. 2013, Chem. Rev., 113, 8710
Balucani, N., Asvany, O., Huang, L. C. L., et al. 2000, ApJ, 545, 892
Balucani, N., Asvany, O., Kaiser, R. I., & Osamura, Y. 2002, J. Phys. Chem. A, 106, 4301
Bester, M., Tanimoto, M., Vowinkel, B., Winnewisser, G., & Yamada, K. 1983, Zeitschrift Naturforschung Teil A, 38, 64
Bester, M., Yamada, K., Winnewisser, G., et al. 1984, A&A, 137, L20
Bouchy, A., Demaison, J., Roussy, G., & Barriol, J. 1973, J. Mol. Struct., 18, 211
Broten, N. W., MacLeod, J. M., Avery, L. W., et al. 1984, ApJ, 276, L25
Carty, D., Le Page, V., Sims, I. R., & Smith, I. W. M. 2001, Chem. Phys. Lett., 344, 310
Cernicharo, J. 1985, Internal IRAM Report (Granada: IRAM)
Cernicharo, J. 2012, in EAS Publications Series, eds. C. Stehlé, C. Joblin, & L. d'Hendecourt, 58 251
Cernicharo, J., & Guelin, M. 1987, A&A, 176, 299
Cernicharo, J., Marcelino, N., Agúndez, M., et al. 2020a, A&A, 642, L8
Cernicharo, J., Marcelino, N., Agúndez, M., et al. 2020b, A&A, 642, L17
Cernicharo, J., Marcelino, N., Pardo, J. R., et al. 2020c, A&A, 641, L9
Chin, Y. N., Kaiser, R. I., Lemme, C., & Henkel, C. 2006, in Astrochemistry – From Laboratory Studies to Astronomical Observations, eds. R. I. Kaiser, P. Bernath, Y. Osamura, S. Petrie, & A. M. Mebel, AIP Conf. Ser., 855, 149
Cuadrado, S., Goicoechea, J. R., Roncero, O., et al. 2016, A&A, 596, L1
Demaison, J., Pohl, I., & Rudolph, H. D. 1985, J. Mol. Spectrosc., 114, 210
de Vicente, P., Bujarrabal, V., Díaz-Pulido, A., et al. 2016, A&A, 589, A74
Fossé, D., Cernicharo, J., Gerin, M., & Cox, P. 2001, ApJ, 552, 168
Goldsmith, P. F., & Langer, W. D. 1999, ApJ, 517, 209
Huang, L. C. L., Balucani, N., Lee, Y. T., Kaiser, R. I., & Osamura, Y. 1999, J. Chem. Phys., 111, 2857
Kaifu, N., Ohishi, M., Kawaguchi, K., et al. 2004, PASJ, 56, 69
Larsson, M., Ehlerding, A., Geppert, W. D., et al. 2005, J. Chem. Phys., 122, 156101
Larsson, M., Geppert, W. D., & Nyman, G. 2012, Rep. Progr. Phys., 75, 066901
Loomis, R. A., Burkhardt, A. M., Shingledecker, C. N., et al. 2021, Nat. Astron., in press, [arXiv:2009.11900]
Lovas, F. J., Remijan, A. J., Hollis, J. M., Jewell, P. R., & Snyder, L. E. 2006, ApJ, 637, L37
Marcelino, N., Agúndez, M., Tercero, B., et al. 2020, A&A, 643, L6
McCarthy, M. C., Lee, K. L. K., Loomis, R. A., et al. 2021, Nat. Astron., in press [arXiv:2009.13546]
McElroy, D., Walsh, C., Markwick, A. J., et al. 2013, A&A, 550, A36
McGuire, B. A., Burkhardt, A. M., Kalenskii, S., et al. 2018, Science, 359, 202
McGuire, B. A., Burkhardt, A. M., Loomis, R. A., et al. 2020, ApJ, 900, L10
McNaughton, D., Romeril, N. G., Lappert, M. F., & Kroto, H. W. 1988, J. Mol. Spectrosc., 132, 407
Moïses, A., Boucher, D., Burie, J., Demaison, J., & Dubrulle, A. 1982, J. Mol. Spectrosc., 92, 497
Pardo, J. R., Cernicharo, J., & Serabyn, E. 2001, IEEE Trans. Antennas Propag., 49, 1683
Quan, D., & Herbst, E. 2007, A&A, 474, 521
Schwahn, G., Schieder, R., Bester, M., & Winnewisser, G. 1986, J. Mol. Spectrosc., 116, 263
Tercero, B., Cernicharo, J., Cuadrado, S., de Vicente, P., & Guélin, M. 2020, A&A, 636, L7
Tercero, F., López-Pérez, J. A., Gallego, J. D., et al. 2021, A&A, 645, A37

Appendix A: Additional table and figures

Table A.1. Observed lines of C_4H_3N isomers towards TMC-1 (CP).

Transition $(J_{K_a,K_c})_u-(J_{K_a,K_c})_l$	Rest freq. (MHz)	E_{up} (K)	A_{ij} (10^{-6} s^{-1})	S_{ij}	$\int T_A^* dv$ (K km s^{-1})	V_{LSR} (km s^{-1})	Δv (km s^{-1})	T_A^* (K)
HCCCH$_2$CN, a-type, μ_a = 2.87 D								
$6_{1,6}-5_{1,5}$	31848.982(3)	6.2	1.39	5.83	0.0093(10)	5.83(2)	0.79(6)	0.0111(8)
$6_{0,6}-5_{0,5}$	32722.702(3)	5.5	1.55	5.99	0.0099(5)	5.67(1)	0.78(3)	0.0120(4)
$6_{2,5}-5_{2,4}$	32876.187(3)	8.8	1.40	5.33	0.0025(6)	5.51(6)	0.66(14)	0.0036(5)
$6_{2,4}-5_{2,3}$	33048.726(3)	8.8	1.42	5.33	0.0016(6)	5.49(10)	0.70(20)	0.0021(5)
$6_{1,5}-5_{1,4}$	33863.716(3)	6.5	1.67	5.83	0.0072(5)	5.66(2)	0.79(4)	0.0085(4)
$7_{1,7}-6_{1,6}$	37139.207(4)	8.0	2.24	6.86	0.0081(5)	5.74(2)	0.69(3)	0.0110(5)
$7_{0,7}-6_{0,6}$	38102.698(4)	7.3	2.47	6.99	0.0110(6)	5.70(1)	0.74(3)	0.0140(5)
$7_{2,6}-6_{2,5}$	38342.339(4)	10.6	2.32	6.43	0.0016(6)	5.56(9)	0.57(18)	0.0027(7)
$7_{2,5}-6_{2,4}$	38616.702(4)	10.7	2.37	6.43	0.0039(5)	5.64(3)	0.60(5)	0.0061(6)
$7_{1,6}-6_{1,5}$	39486.580(4)	8.4	2.70	6.86	0.0075(5)	5.66(2)	0.60(3)	0.0117(6)
$8_{1,8}-7_{1,7}$	42421.779(4)	10.0	3.39	7.87	0.0077(8)	5.74(2)	0.59(5)	0.0122(9)
$8_{0,8}-7_{0,7}$	43450.742(4)	9.4	3.70	7.99	0.0109(11)	5.73(2)	0.73(5)	0.0140(10)
$8_{2,7}-7_{2,6}$	43802.419(4)	12.7	3.55	7.50	0.0028(8)	5.69(4)	0.48(10)	0.0056(10)
$8_{2,6}-7_{2,5}$	44210.195(4)	12.8	3.66	7.50	0.0018(16)	5.70(5)	0.35(31)	0.0047(11)
$8_{1,7}-7_{1,6}$	45099.074(4)	10.6	4.07	7.87	0.0125(9)	5.69(1)	0.61(3)	0.0192(10)
$9_{1,9}-8_{1,8}$	47696.032(5)	12.3	4.86	8.89	0.0036(13)	5.74(6)	0.50(13)	0.0068(17)
$9_{0,9}-8_{0,8}$	48764.484(5)	11.8	5.26	8.98	0.0078(16)	5.76(4)	0.63(10)	0.0117(14)
HCCCH$_2$CN, b-type, μ_b = 2.19 D								
$3_{1,3}-2_{0,2}$, F_u-F_l = 3−2	32519.775(3)	2.3	0.49	1.79	0.0031(8)	5.59(9) (*)	1.06(20)	0.0028(5)
$3_{1,3}-2_{0,2}$, F_u-F_l = 2−1	32519.815(3)	2.3	0.46	1.21				
$3_{1,3}-2_{0,2}$, F_u-F_l = 4−3	32519.916(3)	2.3	0.55	2.58	0.0013(4)	5.73(7)	0.58(22)	0.0021(4)
$9_{0,9}-8_{1,8}$, F_u-F_l = 8−7	36933.586(4)	11.8	0.74	4.44	0.0034(17)	5.80(11) (*)	1.16(31)	0.0027(6)
$9_{0,9}-8_{1,8}$, F_u-F_l = 10−9	36933.621(4)	11.8	0.75	5.57				
$9_{0,9}-8_{1,8}$, F_u-F_l = 9−8	36933.800(4)	11.8	0.74	4.98	0.0020(8)	5.86(12)	0.84(20)	0.0023(6)
$4_{1,4}-3_{0,3}$, F_u-F_l = 4−3	37340.269(4)	3.4	0.77	2.38	0.0025(4)	5.78(7)	0.82(13)	0.0029(6)
$4_{1,4}-3_{0,3}$, F_u-F_l = 3−2	37340.455(4)	3.4	0.75	1.81	0.0030(3)	5.78(4) (*)	0.60(7)	0.0047(5)
$4_{1,4}-3_{0,3}$, F_u-F_l = 5−4	37340.473(4)	3.4	0.82	3.10				
$5_{1,5}-4_{0,4}$, F_u-F_l = 5−4	42010.978(4)	4.6	1.12	2.96	0.0017(5)	5.85(6)	0.46(19)	0.0035(10)
$5_{1,5}-4_{0,4}$, F_u-F_l = 6−5	42011.211(4)	4.6	1.16	3.65	0.0028(13)	5.80(6) (*)	0.54(15)	0.0050(10)
$5_{1,5}-4_{0,4}$, F_u-F_l = 4−3	42011.215(4)	4.6	1.10	2.40				
$6_{1,6}-5_{0,5}$, F_u-F_l = 6−5	46545.801(5)	6.2	1.55	3.57	0.0013(5)	5.63(11)	0.48(20)	0.0026(12)
$6_{1,6}-5_{0,5}$, F_u-F_l = 7−6	46546.045(5)	6.2	1.59	4.24	0.0041(7)	5.69(6) (*)	0.54(9)	0.0071(11)
$6_{1,6}-5_{0,5}$, F_u-F_l = 5−4	46546.057(5)	6.2	1.54	3.00				
CH_2CCHCN, μ_a = 4.07 D								
$6_{1,5}-5_{1,4}$	31615.627(5)	6.4	2.73	5.83	0.0247(12)	5.64(1)	0.80(3)	0.0289(9)
$7_{1,7}-6_{1,6}$	35379.044(5)	7.9	3.90	6.86	0.0213(6)	5.68(1)	0.77(2)	0.0259(5)
$7_{0,7}-6_{0,6}$	36064.688(5)	6.9	4.22	7.00	0.0253(4)	5.64(1)	0.69(1)	0.0347(4)
$7_{2,6}-6_{2,5}$	36140.273(5)	11.4	3.90	6.43	0.0086(8)	5.61(3)	0.90(6)	0.0090(6)
$7_{2,5}-6_{2,4}$	36222.501(5)	11.4	3.93	6.43	0.0095(6)	5.63(2)	0.90(4)	0.0099(5)
$7_{1,6}-6_{1,5}$	36878.547(5)	8.2	4.42	6.86	0.0226(5)	5.63(1)	0.70(1)	0.0300(5)
$8_{1,8}-7_{1,7}$	40425.712(6)	9.9	5.90	7.87	0.0198(8)	5.70(1)	0.60(2)	0.0311(8)

Notes. (*)LSR velocity corresponds to the strongest hyperfine transition. Numbers in parentheses indicate the uncertainty in units of the last significant digits. For the observational parameters we adopted the uncertainty of the Gaussian fit provided by `GILDAS`. HCCCH$_2$CN: Spectroscopic line parameters were obtained using `MADEX` by fitting the rotational lines reported by Demaison et al. (1985) and McNaughton et al. (1988). Dipole moments are from McNaughton et al. (1988). CH_2CCHCN: Spectroscopic line parameters were obtained using `MADEX` by fitting the rotational lines reported by Bouchy et al. (1973) and Schwahn et al. (1986). Dipole moment is from Bouchy et al. (1973). CH_3CCCN: Spectroscopic line parameters were obtained using `MADEX` by fitting the rotational lines reported by Moïses et al. (1982) and Bester et al. (1983). Rotation constants A and D_k have been assumed to be the same as those of CH_3CN. Some additional data have been taken from the CDMS (`https://cdms.astro.uni-koeln.de/`). Dipole moment is from Bester et al. (1984). Note that the E species is 7.8 K above the A species, and energies for the E species are referred to the lowest energy level (1,1).

Table A.1. continued.

Transition $(J_{K_a,K_c})_u-(J_{K_a,K_c})_l$	Rest freq. (MHz)	E_{up} (K)	A_{ij} (10^{-6} s^{-1})	S_{ij}	$\int T_A^* dv$ (K km s^{-1})	V_{LSR} (km s^{-1})	Δv (km s^{-1})	T_A^* (K)
$8_{0,8}-7_{0,7}$	41187.082(6)	8.9	6.34	8.00	0.0245(6)	5.66(1)	0.59(1)	0.0388(7)
$8_{2,7}-7_{2,6}$	41297.656(6)	13.4	5.99	7.50	0.0088(7)	5.67(2)	0.65(4)	0.0128(6)
$8_{2,6}-7_{2,5}$	41420.713(6)	13.4	6.04	7.50	0.0084(7)	5.64(2)	0.65(4)	0.0121(6)
$8_{1,7}-7_{1,6}$	42138.451(6)	10.2	6.68	7.87	0.0194(9)	5.63(1)	0.52(2)	0.0348(10)
$9_{1,9}-8_{1,8}$	45469.519(6)	12.0	8.48	8.89	0.0176(9)	5.69(1)	0.56(2)	0.0293(11)
$9_{0,9}-8_{0,8}$	46297.882(6)	11.1	9.06	9.00	0.0205(11)	5.67(1)	0.55(2)	0.0352(13)
$9_{2,8}-8_{2,7}$	46452.840(6)	15.6	8.70	8.56	0.0097(10)	5.74(2)	0.66(5)	0.0138(10)
$9_{2,7}-8_{2,6}$	46628.069(6)	15.7	8.80	8.56	0.0083(9)	5.64(2)	0.60(4)	0.0129(11)
$9_{1,8}-8_{1,7}$	47394.848(6)	12.5	9.60	8.89	0.0152(13)	5.63(2)	0.62(4)	0.0232(13)
CH_3CCCN, μ_a = 4.75 D								
E 8_2-7_2	33050.3475(8)	29.4	4.18	7.50	0.0044(9)	5.14(9)	1.41(16)	0.0029(5)
E 8_1-7_1	33051.3033(9)	6.9	4.39	7.88	0.0472(8)	5.79(1)	0.76(1)	0.0580(6)
A 8_0-7_0	33051.6219(9)	7.1	4.46	8.00	0.0485(8)	5.80(1)	0.74(1)	0.0616(6)
E 9_2-8_2	37181.5838(9)	31.2	6.08	8.56	0.0013(7)	5.77(10)	0.64(24)	0.0020(7)
E 9_1-8_1	37182.659(1)	8.7	6.32	8.89	0.0421(8)	5.79(1)	0.68(1)	0.0585(7)
A 9_0-8_0	37183.017(1)	8.9	6.40	9.00	0.0455(8)	5.79(1)	0.68(1)	0.0632(7)
E 10_2-9_2	41312.799(1)	33.2	8.46	9.60	0.0025(11)	5.42(8)	0.55(15)	0.0031(10)
E 10_1-9_1	41313.994(1)	10.7	8.73	9.90	0.0372(64)	5.81(4)	0.58(10)	0.0604(9)
A 10_0-9_0	41314.393(1)	10.9	8.81	10.0	0.0412(51)	5.83(3)	0.57(7)	0.0674(9)
E 11_2-10_2	45443.993(1)	35.4	11.4	10.6	...	...	...	≤0.0050(10)
E 11_1-10_1	45445.307(1)	12.9	11.7	10.9	0.0294(42)	5.80(3)	0.57(8)	0.0483(12)
A 11_0-10_0	45445.745(1)	13.1	11.8	11.0	0.0321(42)	5.82(3)	0.62(8)	0.0487(12)
E 12_2-11_2	49575.162(1)	37.7	14.9	11.7	...	...	...	≤0.0060(20)
E 12_1-11_1	49576.596(1)	15.3	15.2	11.9	0.0242(52)	5.75(5)	0.69(14)	0.0328(26)
A 12_0-11_0	49577.073(1)	15.5	15.4	12.0	0.0269(38)	5.81(4)	0.64(8)	0.0393(26)

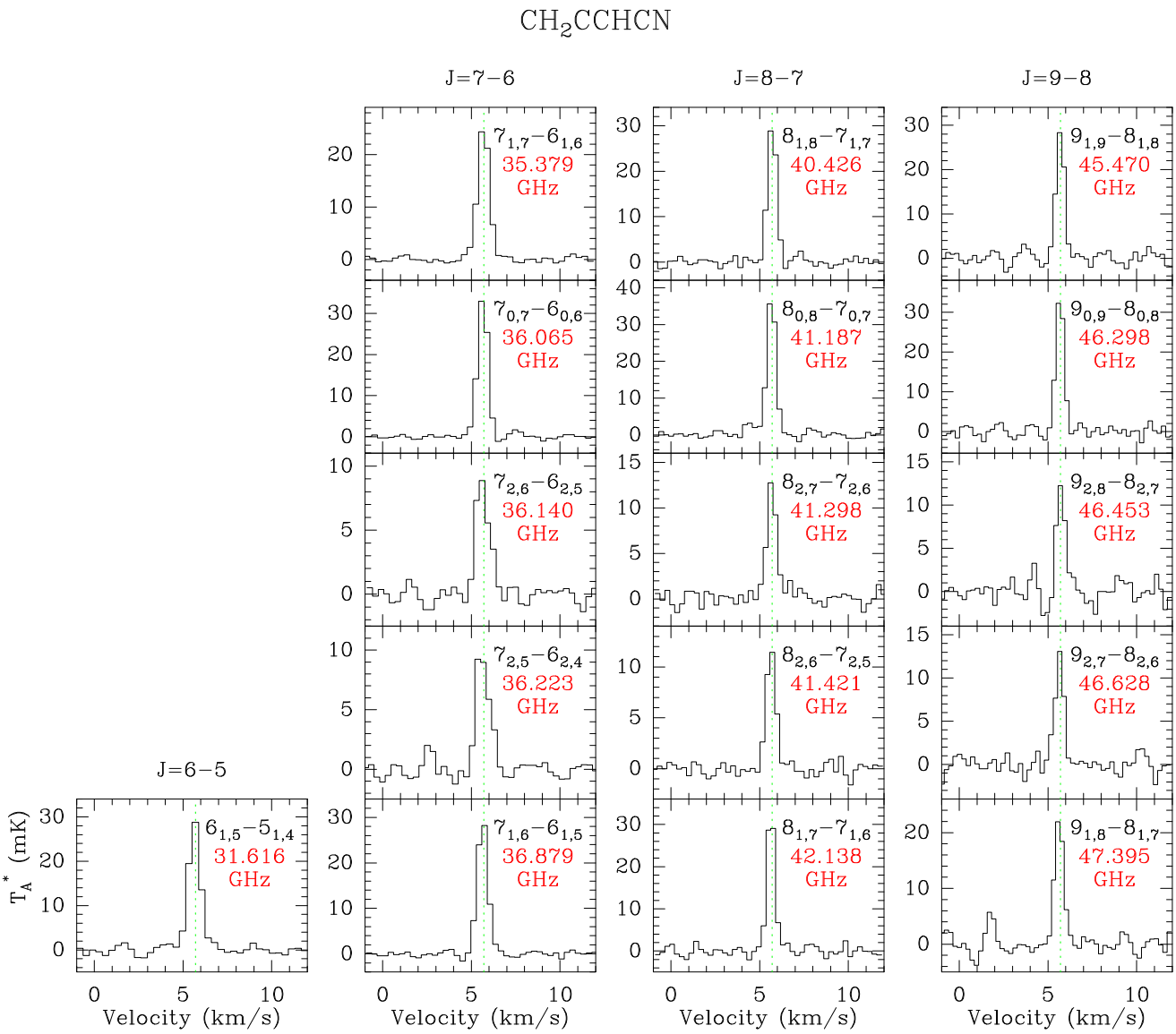

Fig. A.1. Observed lines of CH_2CCHCN towards TMC-1 (CP). The vertical dashed green line marks a radial velocity of 5.7 km s^{-1}.

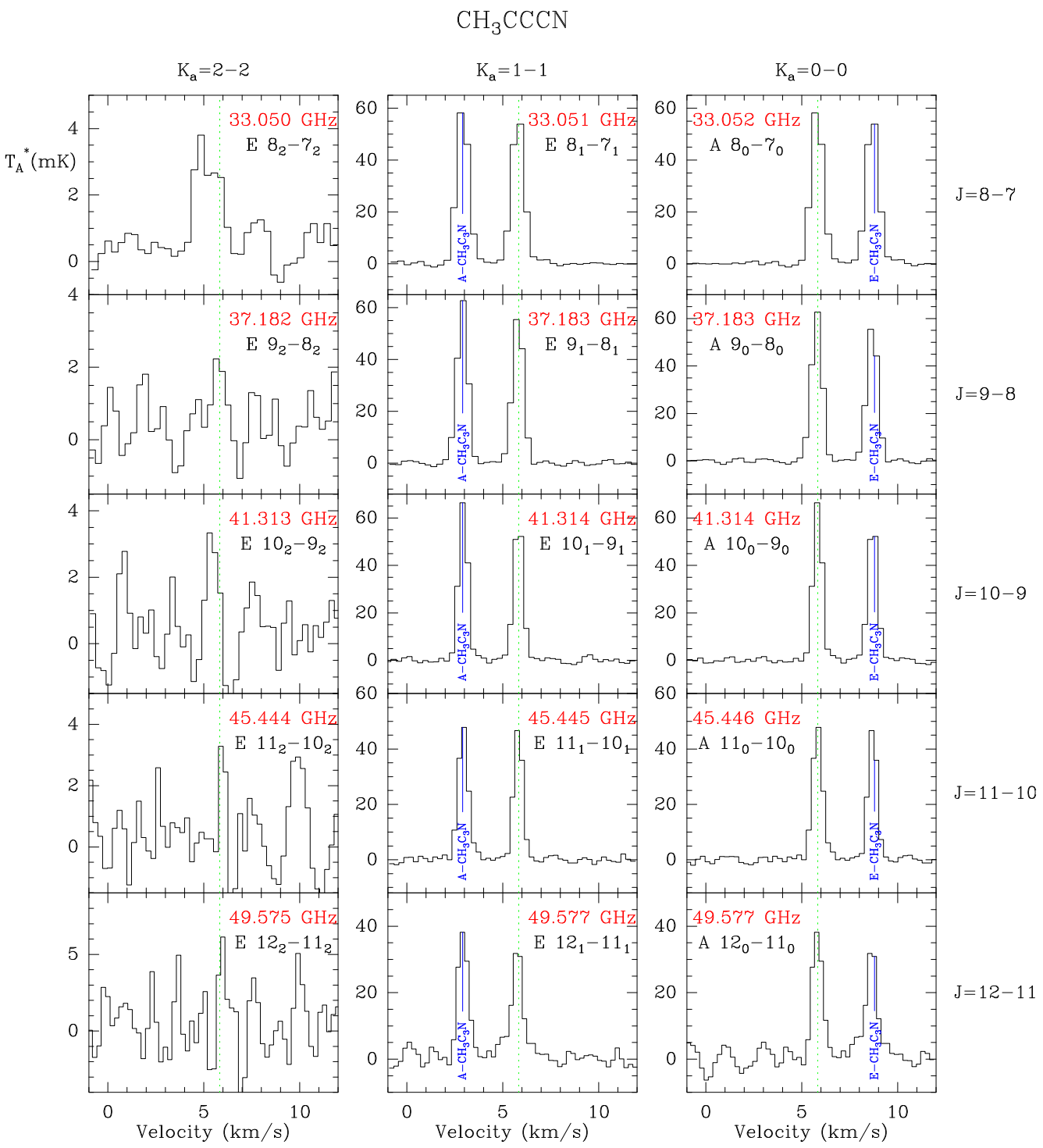

Fig. A.2. Observed lines from CH_3CCCN towards TMC-1 (CP). The dashed green line marks a radial velocity of 5.8 km s^{-1}.

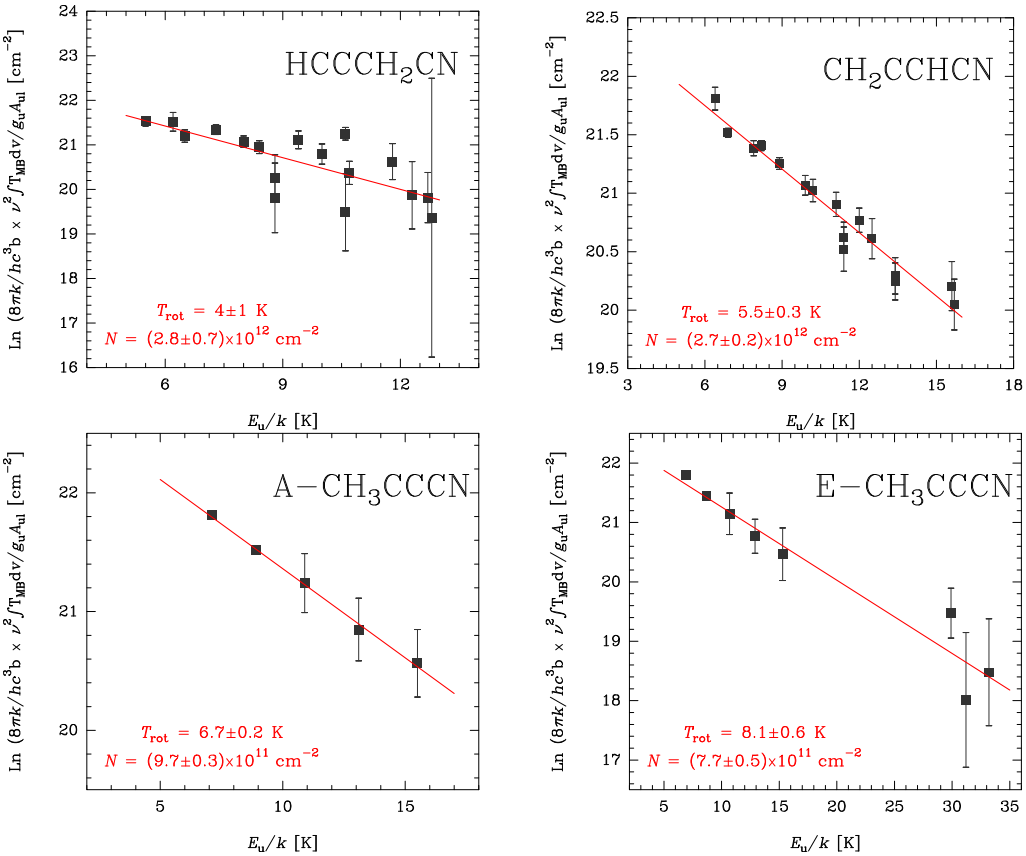

Fig. A.3. Rotational diagrams of the C_4H_3N isomers towards TMC-1 (CP). Derived values of the rotational temperature, T_{rot}, column density, N, and their respective uncertainties are indicated for each molecule.

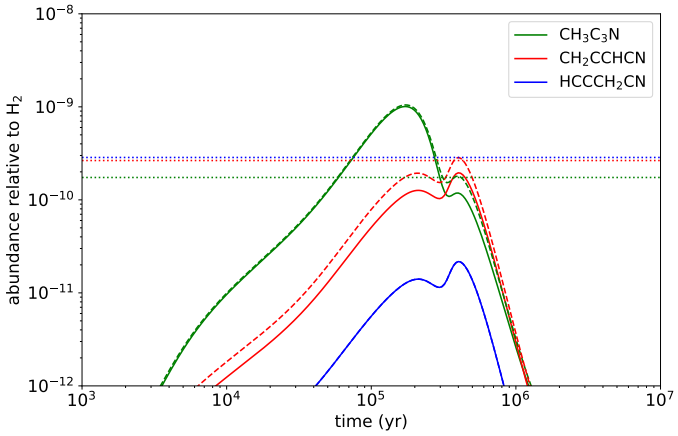

Fig. A.4. Calculated fractional abundances of the three C_4H_3N isomers as a function of time. Solid and dashed lines correspond to two models in which we use branching ratios for the CN + CH_3CCH reaction from Abeysekera et al. (2015) and from Balucani et al. (2000), respectively (see text). The abundances observed in TMC-1 for the three C_4H_3N isomers (from Table 1, adopting an H_2 column density of 10^{22} cm^{-2}; Cernicharo & Guelin 1987) are shown as horizontal dotted lines.

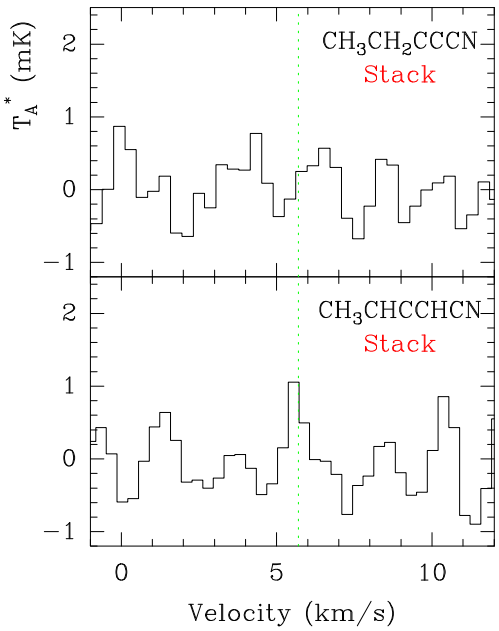

Fig. A.5. Stacked spectra of CH_3CH_2CCCN and $CH_3CHCCHCN$ towards TMC-1.